Materials Horizons

3D Bacterial Flagella as Both Synthetic Biotemplates and Ultrathin Spacers for Enhanced Inter-particle Coupling and Solar Energy Harvesting

Journal:	*Materials Horizons*
Manuscript ID	MH-COM-02-2021-000227.R1
Article Type:	Communication
Date Submitted by the Author:	10-May-2021
Complete List of Authors:	Wang, Lin; University of Oklahoma, Department of Chemistry and Biochemistry Qiu, Penghe; University of Oklahoma, Department of Chemistry & Biochemistry Yang, Tao; Zhejiang University Zhou, Ningyun; University of Oklahoma, Department of Chemistry and Biochemistry zhai, mengmeng; Alliance Pharma Inc, Li, Yan; Zhejiang University Zhou, Yadong; University of Central Florida, Chemistry Zou, Shengli; University of Central Florida, Chemistry Yang, Mingying; Institute of Applied Bioresource Research, College of Animal Science, Zhejiang University Mao, Chuanbin; University of Oklahoma, Department of Chemistry and Biochemistry

New Concepts

We demonstrated a novel concept that biologically-assembled 3D gold nanoparticles (AuNPs) nanochains could efficiently convert solar energy first into heat and then into electricity due to their enhanced plasmonic coupling and broadened solar absorption spectra. Plasmonic nanoparticles, when fabricated or assembled into specific higher-ordered structures, showed great tunability of optical absorption, thus drawn intensive interest in photothermal applications. However, most of the reported structures, mainly 0D and 1D nanomaterials, failed to achieve high solar-thermal energy conversion efficiency. 0D nanoparticles tend to form close-packed patterns during film fabrication, increasing the reflectivity leading to the energy loss. 1D nanochains, although much more favorable for film fabrication, can only absorb strongly in the visible and short-wavelength side of the near infrared range. Besides, the fabrication or assembly of these 1D nanochains is hard to control. Here, ultrathin bionanofibers, bacterial flagella, are used as templates for the 3D arrangement of AuNPs with very small inter-particle gap, allowing enhanced 3D coupling of surface plasmon, which significantly broadened the absorption spectra. As a result, thin films fabricated assembled from the 3D nanochains can serve as a full-spectrum solar absorber and efficiently convert the solar energy into heat that is further turned into electricity in thermoelectric devices.

COMMUNICATION

3D Bacterial Flagella as Both Synthetic Biotemplates and Ultrathin Spacers for Enhanced Inter-particle Coupling and Solar Energy Harvesting

\Received 00th January 20xx,
Accepted 00th January 20xx

DOI: 10.1039/x0xx00000x

Lin Wang,[a,†] Penghe Qiu,[a,†] Tao Yang,[b] Ningyun Zhou,[a] Mengmeng Zhai,[a] Yan Li,[c] Yadong Zhou,[d] Shengli Zou,[d] Mingying Yang[c,*] and Chuanbin Mao[a,b*]

Linear light-absorbing nanomaterials are ideal for film-based solar harvesting applications as they form porous structures that can maximize the absorption and minimize the reflection of the solar light. Conventional 1D nanochains of plasmonic nanoparticle assemblies can achieve significantly broadened optical absorption through surface plasmon coupling, but their optical bands are still not broad enough to absorb through the solar spectrum and thus are not efficient solar absorbers. Here we discovered first by simulation that 3D structured nanochains of plasmonic nanoparticles presented remarkably increased optical broadening effect and much longer redshift of optical peaks due to enhanced inter-particle coupling effect. Then we fabricated the 3D nanochains by assembling gold nanoparticles (AuNPs) around 14 nm ultrathin bionanofibers, the bacterial flagella. The ultrathin biotemplates enabled the 3D arrangement of 50 nm AuNPs along the nanofiber with very small inter-particle gap, allowing the strong coupling of surface plasmon in a 3D manner. Consistent with the theoretical prediction, the 3D nanochains, when assembled into films, could effectively convert nearly the full spectrum of solar energy into heat, which was further efficiently converted into electricity through a thermoelectric generation unit. Our work represents a nanobiomaterial approach to highly efficient solar thermal power generation.

New concepts

We demonstrated a novel concept that biologically-assembled 3D gold nanoparticles (AuNPs) nanochains could efficiently convert solar energy first into heat and then into electricity due to their enhanced plasmonic coupling and broadened solar absorption spectra. Plasmonic nanoparticles, when fabricated or assembled into specific higher-ordered structures, showed great tunability of optical absorption, thus drawn intensive interest in photothermal applications. However, most of the reported structures, mainly 0D and 1D nanomaterials, failed to achieve high solar-thermal energy conversion efficiency. 0D nanoparticles tend to form close-packed patterns during film fabrication, increasing the reflectivity leading to the energy loss. 1D nanochains, although much more favorable for film fabrication, can only absorb strongly in the visible and short-wavelength side of the near infrared range. Besides, the fabrication or assembly of these 1D nanochains is hard to control. Here, ultrathin bionanofibers, bacterial flagella, are used as templates for the 3D arrangement of AuNPs with very small inter-particle gap, allowing enhanced 3D coupling of surface plasmon, which significantly broadened the absorption spectra. As a result, thin films fabricated assembled from the 3D nanochains can serve as a full-spectrum solar absorber and efficiently convert the solar energy into heat that is further turned into electricity in thermoelectric devices.

Introduction

Solar energy, due to its great abundance, long-term sustainability and easy accessibility, has been considered as the most appealing renewable energy resource. As one of the solar energy harvesting methods, solar-thermal conversion has been demonstrated useful in many applications especially solar thermoelectric generation. The effective solar radiation is mainly distributed in the 400-2200 nm range. Thus, for solar energy conversion, optimal solar absorbers should possess intensive optical absorption throughout the whole solar wavelength range. One-dimensional (1D) linear structures are ideal candidates for the fabrication of thin film based solar absorbers, the primary form of its kind in solar applications.

[a.] *Department of Chemistry and Biochemistry, Stephenson Life Sciences Research Center, University of Oklahoma, 101 Stephenson Parkway, Norman, Oklahoma 73019-5300, USA.*
[b.] *School of Materials Science and Engineering, Zhejiang University, Hangzhou, Zhejiang 310027, China.*
[c.] *Institute of Applied Bioresource Research, College of Animal Science, Zhejiang University, Yuhangtang Road 866, Hangzhou, Zhejiang 310058, China.*
[d.] *Department of Chemistry, University of Central Florida, Orlando, Florida 32816, United States.*
† Contribute equally to the work.
*E-mail: maophage@gmail.com; yangm@zju.edu.cn
Electronic Supplementary Information (ESI) available: [details of any supplementary information available should be included here]. See DOI: 10.1039/x0xx00000x

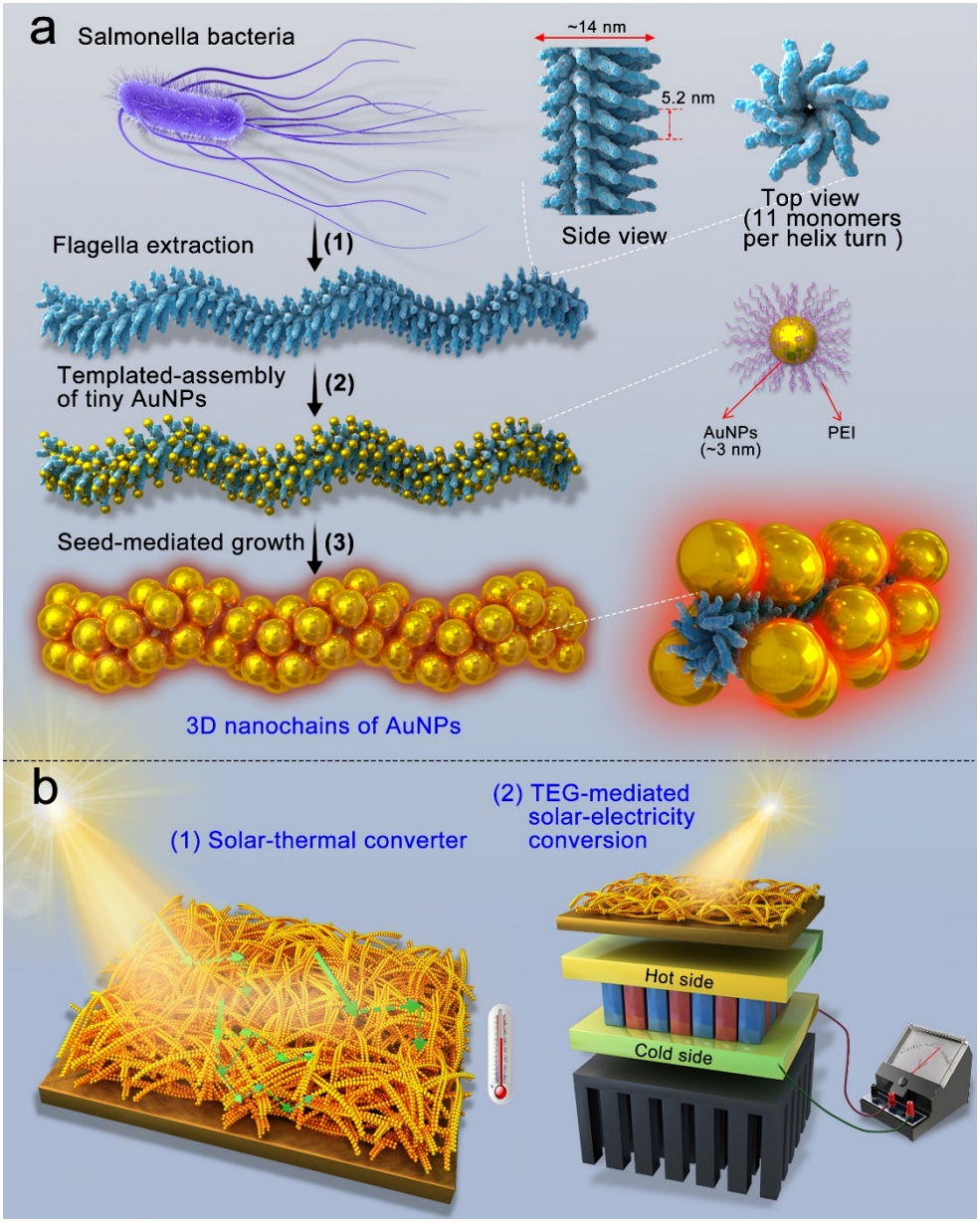

Scheme 1. Fabrication of bacterial flagella-templated 3D Au nanochains with broad optical absorption for solar-thermal energy conversion and electricity generation. a) Fabrication of 3D Au nanochains. (1) and insets: structure of bacterial flagella. Flagella are the motion organ of bacteria. Structurally, they are bio-nanofibers of 14 nm diameter, helically self-assembled from flagellin unit protein. (2) and inset: 3D assembly of tiny 3 nm AuNPs onto flagella nanofiber template through electrostatic interaction between flagella and PEI-coated AuNPs. Due to the distinct size difference, 3 nm AuNPs form a loose 3D linear distribution along the 14 nm flagella template. (3) and inset: 3D black Au nanochains formed through seed-mediated growth of the 3 nm AuNPs on the flagella. During seeded growth, the size of the AuNPs on the flagella template has increased from 3 nm to around 50 nm, resulting in a closely stacked 3D Au nanochains. Due to the small inter-particle gap, strong plasmon coupling takes place among 3D distributed AuNPs not only along the longitudinal direction (like regular 1D nanochains), but also through the transverse direction (unique for the 3D structured nanochains), leading to significantly broadened optical absorption. b) Application of 3D Au nanochains as thin film solar absorber for solar-thermal conversion and electricity generation. (1) Upon deposition onto a copper plate, the 3D nanochains formed a mesoporous, dark black colored thin film. The broad optical band of the 3D nanochains ensures full-spectrum solar absorption and thus high-efficiency solar-thermal conversion. Moreover, the mesoporous structure of the film effectively traps light by multiple internal reflection and absorption (blue arrows), minimizing the reflection loss of the solar radiation. (2) Integration of the 3D nanochain-based thin film solar absorber with a commercial thermal electricity generation (TEG) unit to demonstrate electricity generation using the solar-thermal energy produced by the 3D nanochain film.

Thin films formed by 1D nanomaterials feature porous structures and therefore can effectively trap light through multiple reflection and absorption inside the pores, minimizing the reflection loss of the incident light to the environment. Self or induced assembly of plasmonic nanoparticles, such as gold, silver, copper or aluminum nanoparticles, has provided a simple way of fabricating various types of novel nanostructures.[1-4] More importantly, this method endows great optical tunability to the nanomaterials, which sometimes can hardly be achieved through direct chemical synthesis.[1-7] 1D linear nanochains composed of gold nanoparticles (AuNPs), are one of the most investigated assemblies, with numerous reports on their fabrication, optical properties and applications.[8-17] A significant redshift and broadening of the optical band can be observed upon assembly of spherical AuNPs into 1D linear nanochains,

enabling them for applications demanding optical absorption in the near infrared range, such as solar energy conversion.

The linear structure of the 1D Au nanochains brings them a significant advantage over those zero-dimensional (0D) AuNPs, such as gold nanoshells,[18] nanodendrites,[19, 20] and self-assembled gold clusters and vesicles,[21, 22] which are also potential solar absorbers due to their relatively broad optical absorption. However, 0D nanoparticles tend to form a close-packed pattern during film fabrication, making the films remarkably more reflective.[23-26] Most of the reported 1D linear gold nanochains can indeed absorb strongly in the visible and short-wavelength side of the near infrared range, however, they can rarely capture long-wavelength light in the solar spectrum (i.e. 1100-2200 nm). Failure to collect the full solar radiation is one of the reasons leading to low solar energy conversion efficiency in the current industry. Unlike most of the previously reported nanochains, which were a single string of individual NPs (Fig. 1a), here we hired microorganisms to produce novel nanochains made of AuNPs closely stacked in 3D around a filamentous biotemplate (termed 3D nanochains) (Scheme 1). Specifically, we used bacteria to produce protein nanofibers (~14 nm in diameter), flagella, which are the bacteria-swimming machines attached to the bacterial surface and can be purified by a simple vortexing process. Then we employed the flagella as 1D biotemplates to produce 3D nanochains from AuNPs. The resultant nanochains bear both multiple AuNPs transversely and many AuNPs longitudinally, and can be pictured as close stacking of multiple single NPs strings (Fig. 1c).

This study was motivated by our effort in computational simulation, where we introduced such 3D features into the 3D nanochains and found that the resultant optical spectra were apparently broadened and red-shifted to far NIR region. Then we developed a novel strategy to fabricate the 3D nanochains through the flagella-templated assembly (and the subsequent growth of the assembled AuNPs) of tiny AuNPs (~ 3 nm). Namely, the flagella-templated assembly of the pre-synthesized AuNPs resulted in a loose and scattered 3D distribution of AuNPs along the cylindrical outer wall of the templates. Following a seed-mediated growth process, the individual AuNPs on the templates became larger (up to 50 nm) and simultaneously the inter-particle distance was gradually reduced, to finally form 3D nanochains. The 3D nanochains exhibited an intensive flat optical band throughout a broad range, rendering them an ideal candidate for solar energy harvesting. We then deposited the 3D nanochains onto a copper plate to form a mesoporous dark black thin film. The fabricated film showed a very high solar-thermal conversion efficiency. Finally, we integrated the film into a commercial thermoelectric generation (TEG) unit, and demonstrated that such plasmonic thin films can be used for efficient solar-thermoelectricity generation.

Results and discussion

Computational simulation of the optical spectra of 3D AuNPs nanochains

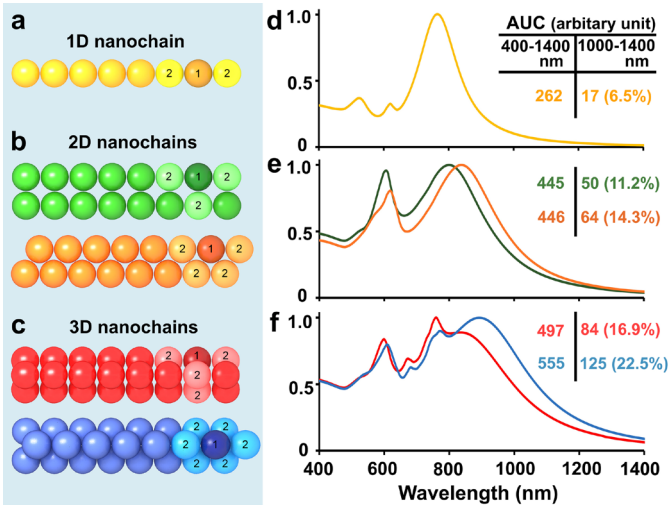

Figure 1. Proposed structures of 1D, 2D and 3D nanochains of 50 nm AuNPs (a-c) and their corresponding simulated optical spectra (d-f, each pair of structure and spectrum shares the same color). A single 1D nanochain is composed of 8 individual 50 nm AuNPs with a uniform inter-particle gap of 1 nm. 2D and 3D nanochains are composed of 2 and 3 single 1D nanochains, respectively. The detailed arrangement is highlighted in different colors on the right end of each nanochains: when any arbitrary AuNP (the darker colored one, labeled with 1) is chosen as the center, then all the surrounding lighter colored AuNPs (labeled 2) have an inter-particle gap of 1 nm to the center AuNPs. Insets in the spectra: left column) the overall area under the curve (AUC) of each spectrum in 400-1400 nm range; right column) the AUC in the 1000-1400 nm range and its percentage in the AUC of the overall spectrum (in the bracket).

We first simulated the optical properties of three model nanochains built from the 50 nm spherical AuNPs, including the 1D nanochain (i.e., a single string of 8 individual AuNPs, Fig. 1a), 2D nanochain (i.e., made of two side-by-side 1D nanochains, Fig. 1b) and 3D nanochain (i.e., composed of three stacked 1D nanochains, Fig. 1c). The inter-particle spacing among the nearest AuNPs is 1 nm in all nanochains. The simulations were carried out using the discrete dipole approximation (DDA) and T-Matrix method.[27, 28] The dielectric constants of Au were taken from Palik's handbook.[29] Fig. 1 shows the normalized simulated spectra of the typical possible arrangements of NPs in each type of nanochains. Generally, the absorption bands were apparently broadened and red-shifted along with the increasing dimension of nanochains. By normalizing each spectrum at its highest peak intensity, the area under the curve (AUC) can be used to evaluate mathematically the broadness and the absorption intensity of a spectrum within a certain wavelength range. The AUC of each spectrum within the overall 400-1400 nm range has increased as much as 70.2% and 111.8% for 2D and 3D nanochains respectively, comparing to that of the 1D nanochains, suggesting a significant broadening of optical bands in a transition from 1D to 3D nanochains (Fig. 1 d-f). The AUC in the longer wavelength range, i.e. 1000-1400 nm in this case, can reflect the redshift of the spectrum. The AUC within the 1000-1400 nm range was merely 17 for 1D nanochains, but reached up to 64 for 2D nanochains and 125 for 3D nanochains, equivalent to 6.5%, 14.3% and 22.5% of their corresponding overall AUC. Both the remarkably increased AUC values and their weight in the overall AUC confirmed the redshift of the optical bands as a result of increased nanochains dimensions. In addition, two types of NP stacking were studied in both 2D and

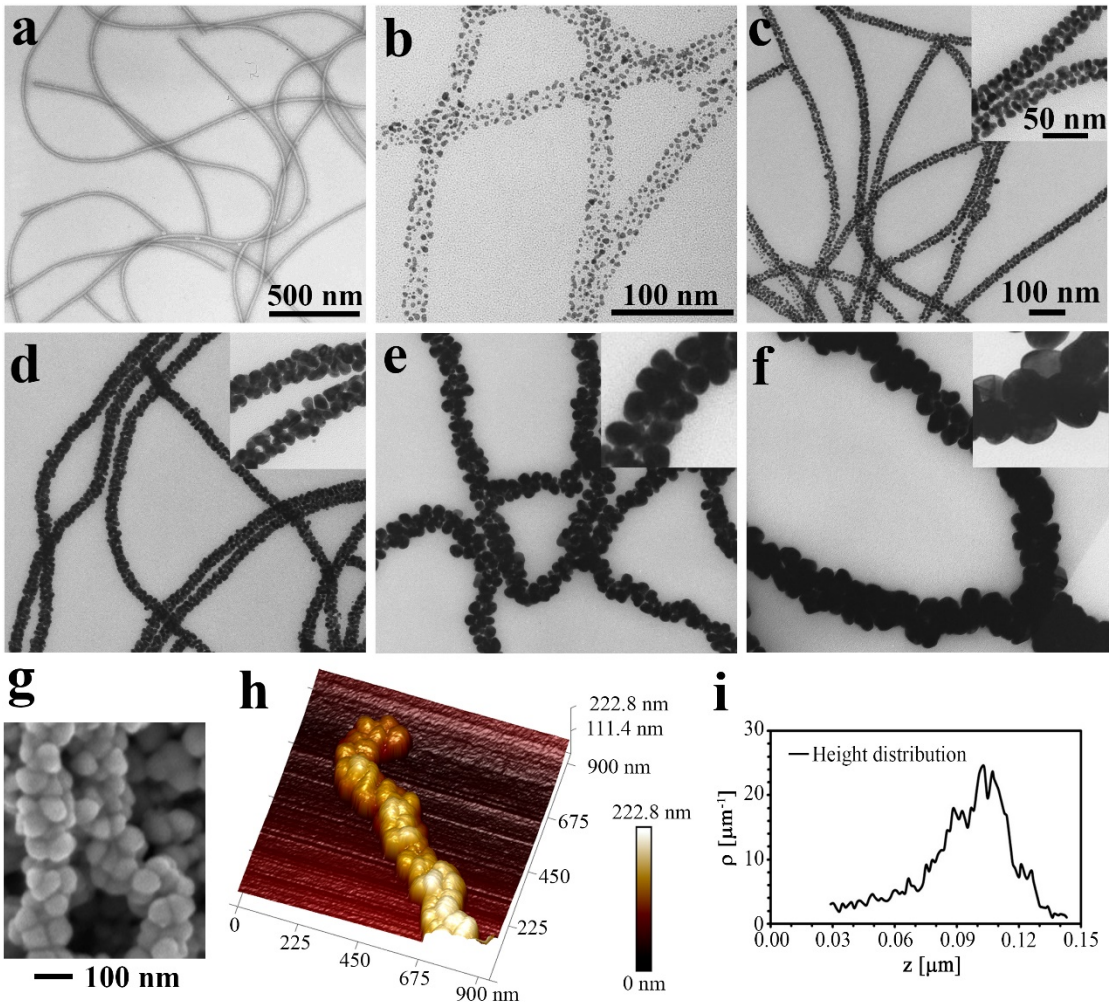

Figure 2. 3D nanochains of AuNPs fabricated by bionanofibrous flagella templates. a) TEM image of the flagella bionanofibers (14 nm wide), negatively stained with uranyl acetate (1%). b) TEM image of 3D scattered assembly of pre-synthesized ~3 nm AuNPs onto the cylindrical outer wall of the flagella templates. c-f) TEM image showing seed-mediated growth of the AuNPs on the 3D nanochains to reach an average AuNPs size of 8 nm (c), 14 nm (d), 28 nm (e), and 50 nm (f), respectively. The enlargement of AuNPs size was also associated with simultaneous decrease of inter-particle distance. When the AuNPs reached 50 nm, the inter-particle distance was so small that the overall nanochains appeared to be made of closely stacked AuNPs, structurally similar to the sketch of 3D nanochains in Fig. 1c. g-h) SEM (g) and AFM (h) characterization of the 3D structure of the nanochains composed of 50 nm AuNPs. The two images show that AuNPs in the nanochains were closely stacked in a 3D manner (g & h). (i) The height distribution plot extracted from the AFM image in h. z indicates height, and ρ indicates the density of data points on the nanochain at each height z values. The height distribution indicates that there are mainly two layers of AuNPs in a single nanochain (Fig. 1c). c-f share the same scale bars as c (100 nm for the main image and 50 nm for its inset). No negative staining was applied to samples in b-f.

3D nanochains models (upper and lower panel in Figure 1b and 1c, illustrating less and more closely stacked pattern, respectively). Each AuNP in the lower panel has more adjacent NPs with 1 nm gap than that in the upper panel (Fig. 1b & c). Based on the AUC values and their weight for two different stacking patterns in both 2D and 3D models, the more densely the NPs were compacted (lower panel in each model), the more broaden and red shifted the spectrum was (Fig. 1e & f). Such a phenomenon should hold true on AuNPs arrays of other NPs sizes and inter-particle distances, although the degree of broadening and redshift may vary due to the size- and distance-dependent nature of plasmon coupling.

Fabrication and characterization of 3D AuNPs nanochains

Currently, fabrication of AuNPs nanochains is achieved mainly through induced self-assembly of pre-synthesized NPs, which usually results in 1D nanochains. Direct preparation of 2D and 3D nanochains through self-assembly of AuNPs has been very challenging. The only few examples in the literature are limited by extremely large inter-particle distance or impurity and non-scalable production issues.[12, 30] Here, instead of inducing the self-assembly of AuNPs, we employed a templated-assembly strategy followed by a seed-mediated growth procedure to fabricate 3D nanochains. We first purified flagella (14 nm in diameter and up to 20 μm in length, Fig. 2a) from wild type Salmonella Typhimurium bacteria following our reported protocol.[31-33] We then used them as templates to first assemble tiny AuNPs (~ 3 nm, Fig. S1) into a loosely scattered 3D distribution of NPs along the cylindrical outer wall of the templates (Fig. 2b). The flagella are naturally assembled from anionic protein subunits (called flagellin) by bacteria and thus could electrostatically assemble the AuNPs coated by cationic polyethyleneimine (PEI). Then we conducted a single-step seed-mediated growth process, in which the tiny AuNPs on the

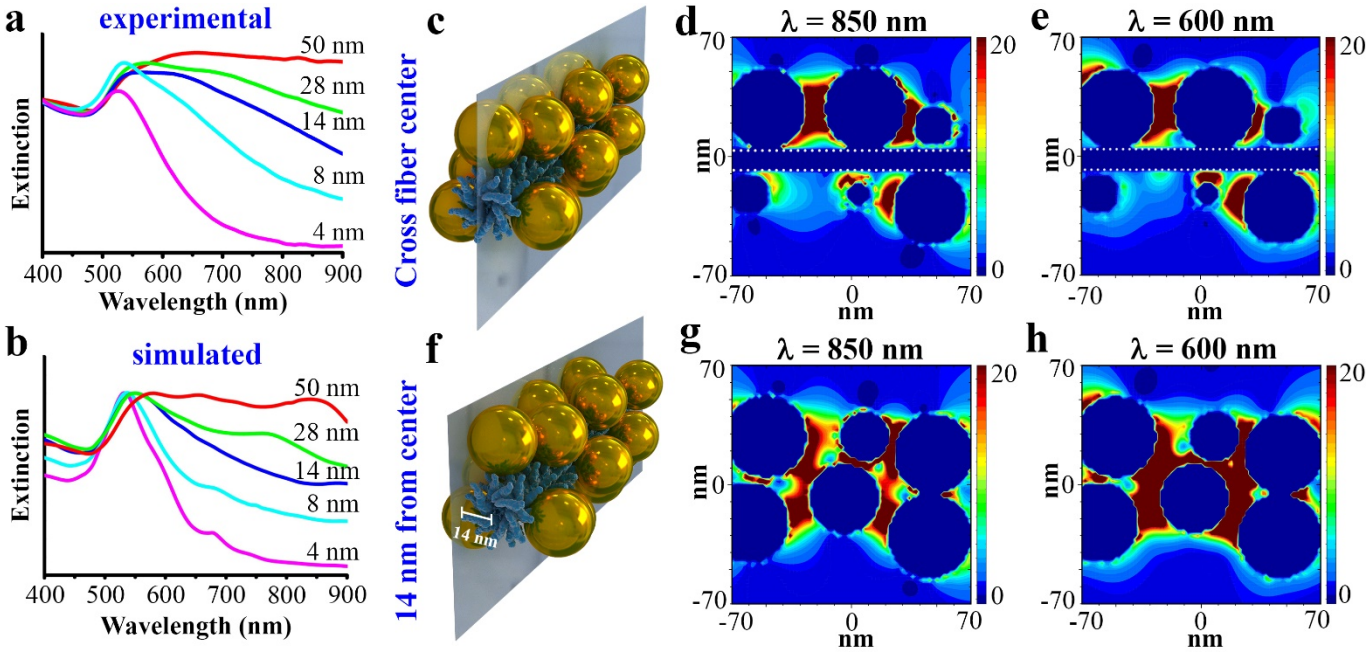

Figure 3. Optical properties of the flagella templated 3D AuNPs nanochains. a &b) Measured (a) and the corresponding simulated (b) extinction spectra of the 3D nanochains shown in Figs. 2b-2f, the average AuNPs size on the nanochains is 4, 8, 14, 28 and 50 nm respectively; c-h) Simulated electric field |E|2 distribution of the 50 nm AuNPs 3D nanochains at cross sections through the center of the fiber (c-e) and 14 nm away from the fiber center (f-h), with an incident light wavelength of 850 nm (d, g) and 600 nm (e, h). c and f depicted the position of the cross sections in the 3D Au nanochains. Due to the 3D structure of the nanochains, it would be practically difficult to show the electric field in the transverse direction, thus longitudinal sectional view right through the template and 14 nm away from the template were adopted to show the 3D electric field distribution along the nanochains. Please note the nanochain was constructed by uniform 50 nm AuNPs, the size difference of their cross sections in d, e, g, h is due to the 3D distribution of the AuNPs along the fiber, which also made the inter-particle spacing appeared significantly larger than their actual value in 3D space. The spacing between two white dashed lines in d and e indicates the position of flagella.

flagella templates acted as seeds, to obtain 3D linear arrays of larger AuNPs. By manipulation of the ratio between the seeds on flagella and $HAuCl_4$, the size of the resultant AuNPs were well controlled (Fig. 2c-f). Along with the increasing size of the AuNPs, the inter-particle distance gradually reduced. When the size of AuNPs reached about 50 nm, we obtained 3D nanochains composed of closely stacked AuNPs (Fig. 2f). It should be noted that throughout the seeded growth of AuNPs on flagella from 3 nm to 50 nm, there was no apparent fusion of neighboring NPs and individual AuNPs could be still clearly identified at all sizes. Moreover, the density of AuNPs, defined as the number of AuNPs in a unit length of the flagella template, was significantly reduced with the increasing size of AuNPs (inset, Fig. 2c-f). We believe that when the gap between two neighboring AuNPs is reduced to a critical size, as a result of the seeded growth, coalescence of AuNPs will take place to fuse and rearrange smaller NPs to larger ones,[34-36] which may possibly account for the reduced density of AuNPs on flagella.

We then employed SEM and AFM to characterize the 3D structure of the nanochains. Both the SEM and AFM images showed that all the AuNPs in the nanochains were closely stacked with each other in a 3D manner. With the Gwyddion software, we further isolated the single 50 nm AuNPs nanochain shown in Fig. 2h from the background by setting a height threshold (Fig. S2) and extracted the height (z) distribution of the nanochains (Fig. 2i). It can be seen that the height of the nanochains mainly spans from 60 to 120 nm, with the peak distribution in the 100-110 nm range (Fig. 2i). Considering that the average size of AuNPs in the nanochains is around 50 nm and the diameter of the flagella is merely 14 nm, such a height distribution profile must be generated by two layers of AuNPs in the nanochain, stacking in a way similar to the 3D nanochains depicted in Fig. 1c.

The advantages of the nanofibrous flagella templates lie in following several aspects. First, structurally, flagella are highly ordered helical assembly of flagellin protein monomers.[37] Thus they are natively charged with uniform diameter, allowing them to be used directly as templates without the need of surface modification, which is usually a necessary step for other inorganic nanofibers.[38] Such protein assemblies will not interfere the plasmon coupling of metallic NPs assembled on them. Second, the diameter of the flagella used in this work is only around 14 nm, which is optimal for the fabrication of our proposed 3D nanochains. Templates of a larger diameter will take a tremendous amount of space inside the nanochains, weakening the multi-dimensional plasmon coupling of the NPs. However, templates of a smaller diameter may not have sufficient surface area to accommodate densely packed NPs throughout the seeded growth. Moreover, once the nanochains are deposited for device fabrication, just like any biological tissues, the flagella will become flattened (Fig. S3), which will further reduce the inter-particle distance at the transverse direction of the nanochains, resulting in even stronger plasmon coupling of NPs. Flagella still have their uniqueness even when compared to other common biological nanofibers, such as filamentous phage, tobacco mosaic virus (TMV), and DNA assemblies. For example, TMV and filamentous phage are less than 1 μm in length. Thus, they are not ideal for the fabrication

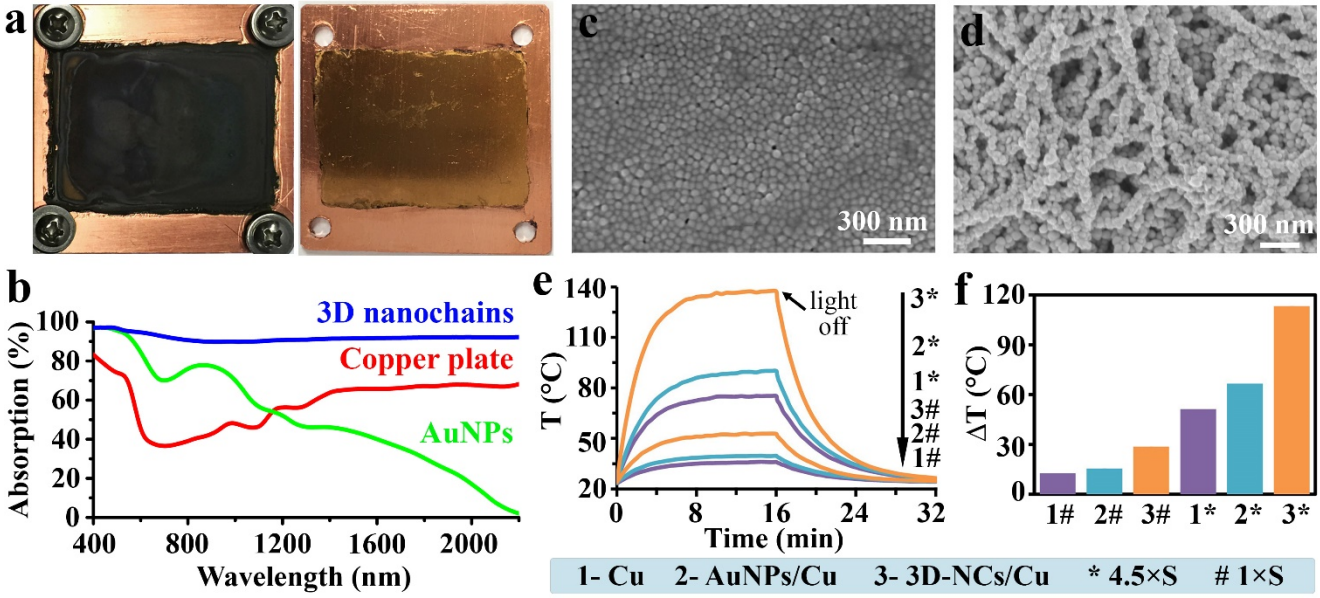

Figure 4. 3D Au nanochains films for solar-thermal conversion. a) Photographs of 3D Au nanochains film (left) and AuNPs film (right) deposited on the copper plates. b) Absorption spectra of the films made of 3D Au nanochains and AuNPs as well as the copper plate used to support the films. c&d) SEM images of the AuNPs film (c) and the nanochains film (d); e) Temperature profile of the films over the time irradiated by simulated sunlight with a power density 1 time (1xS) or 4.5 times (4.5xS) of that of the natural sunlight; f) Plot of the temperature increase (ΔT=T16min-T0min) for each film derived from the temperature profile in e. Cu, copper plate; AuNPs/Cu, free AuNPs film coated on the copper plate; 3D-NCs/Cu, 3D Au nanochains film coated on the copper plate.

of porous thin films, which are essential to achieve high-efficiency solar absorption (as discussed later).[39, 40] The natural double stranded DNA is too narrow to hold the 3D NPs onto them.[41-43] While DNA origami are very promising to generate nanofibers similar to flagella, the effort and the cost to obtain such artificial nanofibers are not comparable to those of the naturally produced flagella.

Optical properties of 3D AuNPs nanochains

Our flagella- templated and seeded growth strategy also allows us to fine tune the optical property of the AuNPs/flagella assemblies. The alteration of optical properties can be easily observed by color changes of the post-grown solutions, which turned to light red, light purple, dark purple and greyish black, respectively, when different ratios between the seeds on flagella and $HAuCl_4$ were applied to increase the AuNPs size (Fig. S4, corresponding to the structures in Figs. 2c-f respectively). The optical extinction spectra of the 3D nanochains (Fig. 3a) showed that with increasing AuNPs size and decreasing inter-particle distance, the optical bands became increasingly broadened, and finally became flattened over a long wavelength range when AuNPs reached 50 nm. The measured spectrum of our synthesized 3D nanochains (Fig. 3a, red curve) was even broader in the collected wavelength range than the optical spectra of the simulated 50 nm AuNPs chains (Fig. 1f). We attributed such a difference to the randomized inter-particle distance as a result of the seeded growth of AuNPs on the flagella templates.

To confirm this, we further simulated the optical spectra of our synthesized 3D nanochains using the DDA method.[27] In the simulations, model nanochains were built by randomly generating AuNPs with a defined size and density on the surface of a 14 nm fiber, which represents the flagella template (see supplementary information for details). The density of AuNPs was roughly estimated from the AFM images and the corresponding height profiles. With this random model, we were able to obtain optical spectra of 3D nanochains matching quite well to the measured ones (Fig. 3b). The electric field $|E|^2$ distribution on the nanochains were also studied using the 50 nm AuNPs nanochains. In the simulations, we calculated the electric field contour plots through the center of the fibers and 14 nm away from the centers (Figs. 3d, e, g and h). We also calculated electric fields at both 600 and 850 nm wavelength. From the contour plots, we may see that enhanced local fields can be found at both planes and wavelengths. The simulations suggest that the strong coupling can be obtained at different wavelengths, and nanoparticles at different locations (both along longitudinal and transverse directions) also couple with each other strongly. This can be found in the electric field contour plots at the planes through the fiber centers and 14 nm away from the fiber centers. These two effects collectively led to broad optical extinction of the 3D nanochains in a wide wavelength range.

Efficient solar thermal electricity conversion by 3D AuNPs nanochain films

The broadband optical property makes the 3D nanochains a suitable candidate for solar energy harvesting and conversion. As a demonstration, we fabricated a thin film using the 3D nanochains of 50 nm AuNPs and tested its performance in solar-thermal generation. As shown in Fig. 4a (left), a dark black thin film of about 4.5 cm× 3.3 cm was obtained by air-evaporation of the ethanol solution of the nanochains on an edge-sealed copper plate. A free AuNPs thin film prepared using individually dispersed 50 nm AuNPs (Fig. 4a right and Fig. S5) as well as an unmodified copper plate were employed as controls for the

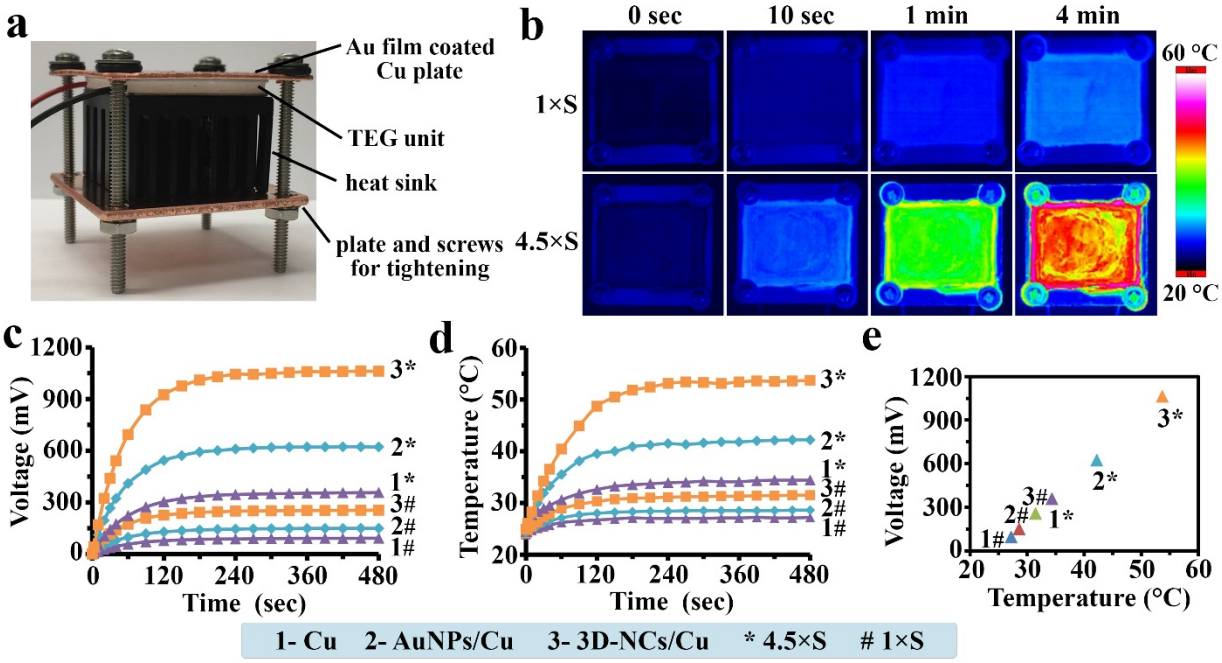

Figure 5. Integration of the 3D nanochains film with a commercial TEG unit for solar-thermal based electricity generation. a) Assembly of the device. b) Infrared camera images of 3D nanochains absorber during irradiation. c-d) Voltage (c) and temperature (d) produced by different films in response to the irradiation of simulated sunlight with a power density 1 time (1xS) or 4.5 times (4.5xS) of that of the natural sunlight. d) Plot of voltage versus absorber temperature at the end point of testing (480 sec). Sample: 1, Cu, copper plate; 2, AuNPs/Cu, pure AuNPs film coated copper plate; 3, 3D-NCs/Cu, 3D Au nanochains film coated copper plate. * and # correspond to power density of 4.5×S and 1×S, respectively.

measurement. The 3D nanochains film had a broadband absorption that covered the whole effective solar spectrum (400-2200 nm), with at least 90% absorption at each wavelength (Fig. 4b). In contrast, the free AuNPs film had much weaker absorption than the 3D nanochains film. Its absorption was dropped to 80% at 620 nm, and further dropped to 70% and 40% at around 1000 nm and 1600 nm, respectively. Under SEM, in the free AuNPs film, the AuNPs were closely packed with the neighboring NPs (Fig. 4c and Fig. S6a), which made the overall film compact and smooth with high reflection, whereas the black nanochains film was mesoporous (Fig. 4d and Fig. S6b). Such porous nanochains film can enhance the absorption of light, as it can effectively trap light to induce multiple internal reflection and absorption inside the pores, with minimum external reflection on the surface of the film.[44, 45]

For solar-thermal conversion test, the copper plates coated by the 3D nanochains film (3D-NCs/Cu) and the free AuNPs film (AuNPs/Cu) as well as the copper plate (Cu) were irradiated by simulated sunlight with a power density 1 time (termed 1S) or 4.5 times (termed 4.5S) of that of the natural sunlight. The temperature of the copper plates was recorded using a surface thermocouple probe during the 16 min irradiation. The actual temperature as well as the temperature increase (ΔT, defined as T_{16min}-T_{0min}) are plotted in Fig. 4e and 4f. With 1S sunlight, the temperature of the nanochains film coated Cu plate could increase to 52.7 °C from 24 °C, resulting in a ΔT value of 28.7 °C, much higher than that of the Cu plate (12.6 °C) and the free AuNPs film (15.6 °C). When 4.5S sunlight was applied, the temperature difference became increasingly larger, and the ΔT could even reach 51.3 °C, 66.6 °C and 113.3 °C for Cu, AuNPs/Cu, and 3D-NCs/Cu plates, respectively. But still, the ΔT for the 3D nanochains film was the highest. The solar-thermal conversion efficiency of the films was also estimated from the temperature profile under both the radiation power of 1S and 4.5S following a published energy balance method.[46] The conversion efficiency of 3D-NCs/Cu could reach approximate 90%, significantly higher than 19% and 42% for Cu and AuNPs/Cu, respectively (Table S1).

To further demonstrate that our 3D nanochains films could be used for electricity generation by absorbing sunlight, we also integrated the above 3D nanochains film coated copper plate directly with a commercial thermoelectric generator (TEG) unit (Figs. 5a & S7) and demonstrated that such a film could be used to generate electricity through solar thermal heat.[47-49] A TEG unit has a hot and a cold side. The hot side is in contact with the solar absorber coated copper plate and the cold side is placed right on top of the heat sink. The sandwich structure was glued together with a thin layer of heat transfer paste. Under irradiation, there would be immediate heat flow from the film to the copper plate and then through the TEG unit to generate electricity. Throughout the simulated solar irradiation, the voltage generated by the device was recorded, and the temperature of the hot side (3D-NCs/Cu, free AuNPs/Cu, and Cu plates) was monitored by both a thermal probe and an infrared camera (Fig. 5b). Surprisingly, both the voltage and the temperature increased rapidly at first and shortly reached a steady state (Figs. 5c & 5d). At the steady state, the solar heat generation and heat transfer to the TEG unit was balanced. The output voltages at the steady state for the device assembled with 3D-NCs/Cu, free AuNPs/Cu and Cu plates were 254.4, 149.5 and 92.0 mV, respectively, under 1S sunlight, and were 1061.0, 622.0 and 356.9 mV under 4.5S sunlight, respectively. The correlation between the output voltage and the

temperature of the hot side (Fig. 5e) suggests that our 3D nanochains films can absorb sunlight effectively and convert solar energy more efficiently into the electricity, resulting in higher temperature increase and subsequently higher output voltage out of the TEG device.

Conclusions

In summary, we have proposed and fabricated a novel type of 3D structured Au nanochains with broadband optical absorption. Our calculations showed that by incorporating 3D features into the nanochains, their optical bands could be significantly broadened compared to the most commonly seen 1D nanochains. Due to the native charges and ultrathin diameter, the nanofibrous flagella biotemplates allowed us to successfully fabricate such 3D nanochains through templated assembly of AuNPs followed by seeded growth. The thin films made of the 3D nanochains can absorb intensely throughout the whole solar spectrum. Such films could harvest solar energy and efficiently convert it into heat. When combined with a commercial TEG unit, our 3D nanochains film could be used to generate electricity through converting the solar-thermal heat into the electricity. Comparing to the currently available solution-processed 0D broadband plasmonic materials, our 3D nanochains are a better option for thin film based solar applications, as the porous film structure formed by the 3D nanochains can effectively enhance the absorption of sunlight and reduce the loss of light through surface reflection. This flagella-templated strategy for fabricating 3D nanochains and porous films is not only limited to gold, but also applicable to other types of plasmonic materials for optical property manipulation and solar energy related applications.

Author Contributions

Lin Wang and Penghe Qiu contribute equally to the work.

Conflicts of interest

There are no conflicts to declare.

Acknowledgements

This work is partially supported by the Office of Basic Energy Sciences within the Department of Energy (DOE) Office of Science (DE-SC0016567). S.Z. acknowledges the Extreme Science and Engineering Discovery Environment (XSEDE) Open Science Grid (OSG) as the service provider through allocation szou. We would like to thank Dr. Xiangming Xiao for providing instrument for spectroscopic measurements.

Notes and references

1. S. G. Park, C. Mun, M. Lee, T. Y. Jeon, H. S. Shim, Y. J. Lee, J. D. Kwon, C. S. Kim and D. H. Kim, *Adv Mater*, 2015, **27**, 4290-4295.
2. H. J. Yang, S. Y. He, H. L. Chen and H. Y. Tuan, *Chemistry of Materials*, 2014, **26**, 1785-1793.
3. L. Zhou, Y. L. Tan, D. X. Ji, B. Zhu, P. Zhang, J. Xu, Q. Q. Gan, Z. F. Yu and J. Zhu, *Sci Adv*, 2016, **2**.
4. L. Zhou, Y. L. Tan, J. Y. Wang, W. C. Xu, Y. Yuan, W. S. Cai, S. N. Zhu and J. Zhu, *Nat Photonics*, 2016, **10**, 393-+.
5. J. A. Fan, C. H. Wu, K. Bao, J. M. Bao, R. Bardhan, N. J. Halas, V. N. Manoharan, P. Nordlander, G. Shvets and F. Capasso, *Science*, 2010, **328**, 1135-1138.
6. N. J. Halas, S. Lal, W.-S. Chang, S. Link and P. Nordlander, *Chemical Reviews*, 2011, **111**, 3913-3961.
7. L. S. Slaughter, B. A. Willingham, W. S. Chang, M. H. Chester, N. Ogden and S. Link, *Nano Lett*, 2012, **12**, 3967-3972.
8. T. H. Chen, M. Pourmand, A. Feizpour, B. Cushman and B. M. Reinhard, *J Phys Chem Lett*, 2013, **4**, 2147-2152.
9. M. Li, S. Johnson, H. T. Guo, E. Dujardin and S. Mann, *Adv Funct Mater*, 2011, **21**, 851-859.
10. Z. H. Nie, D. Fava, E. Kumacheva, S. Zou, G. C. Walker and M. Rubinstein, *Nat Mater*, 2007, **6**, 609-614.
11. S. X. Xing, L. H. Tan, M. X. Yang, M. Pan, Y. B. Lv, Q. H. Tang, Y. H. Yang and H. Y. Chen, *J Mater Chem*, 2009, **19**, 3286-3291.
12. X. S. Shen, L. Y. Chen, D. H. Li, L. F. Zhu, H. Wang, C. C. Liu, Y. Wang, Q. H. Xiong and H. Y. Chen, *Acs Nano*, 2011, **5**, 8426-8433.
13. M. G. Warner and J. E. Hutchison, *Nat Mater*, 2003, **2**, 272-277.
14. S. Lin, M. Li, E. Dujardin, C. Girard and S. Mann, *Adv Mater*, 2005, **17**, 2553-2559.
15. S. A. Maier, M. L. Brongersma, P. G. Kik, S. Meltzer, A. A. G. Requicha and H. A. Atwater, *Adv Mater*, 2001, **13**, 1501-1505.
16. Z. Yin, W. Zhang, Q. Fu, H. Yue, W. Wei, P. Tang, W. J. Li, W. Z. Li, L. L. Lin, G. H. Ma and D. Ma, *Small*, 2014, **10**, 3619-3624.
17. J. Lu, Y.-X. Chang, N.-N. Zhang, Y. Wei, A.-J. Li, J. Tai, Y. Xue, Z.-Y. Wang, Y. Yang, L. Zhao, Z.-Y. Lu and K. Liu, *Acs Nano*, 2017, **11**, 3463-3475.
18. O. Neumann, A. S. Urban, J. Day, S. Lal, P. Nordlander and N. J. Halas, *Acs Nano*, 2013, **7**, 42-49.
19. P. H. Qiu, M. Y. Yang, X. W. Qu, Y. Y. Huai, Y. Zhu and C. B. Mao, *Biomaterials*, 2016, **104**, 138-144.
20. J. J. Zhou, Y. Y. Jiang, S. Hou, P. K. Upputuri, D. Wu, J. C. Li, P. Wang, X. Zhen, M. Pramanik, K. Y. Pu and H. W. Duan, *Acs Nano*, 2018, **12**, 2643-2651.
21. P. Huang, J. Lin, W. W. Li, P. F. Rong, Z. Wang, S. J. Wang, X. P. Wang, X. L. Sun, M. Aronova, G. Niu, R. D. Leapman, Z. H. Nie and X. Y. Chen, *Angew Chem Int Edit*, 2013, **52**, 13958-13964.
22. D. L. Liu, F. Zhou, C. C. Li, T. Zhang, H. H. Zhang, W. P. Cai and Y. Li, *Angew Chem Int Edit*, 2015, **54**, 9596-9600.
23. R. R. Qin, Y. C. Liu, F. Tao, C. Li, W. F. Cao and P. Yang, *Adv Mater*, 2019, **31**, 1803377.
24. M. Zaier, L. Vidal, S. Hajjar-Garreau and L. Balan, *Sci Rep-Uk*, 2017, **7**, 12410.
25. Y.-K. Park and S. Park, *Chemistry of Materials*, 2008, **20**, 2388-2393.
26. L. Minati, A. Chiappini, F. Benetti, G. Speranza, D. Zonta, A. Piotrowska, M. Marciniak, A. Vaccari and M. Ferrari, *Colloids Surf., A*, 2015, **482**, 431-437.

27. B. T. Draine and P. J. Flatau, *J. Opt. Soc. Am. A*, 1994, **11**, 1491-1499.
28. D. W. Mackowski, *J. Opt. Soc. Am. A*, 1994, **11**, 2851-2861.
29. E. D. Palik, *Handbook of Optical Constants of Solids*, Academic Press, 1998.
30. H. Wang, L. Y. Chen, X. S. Shen, L. F. Zhu, J. T. He and H. Y. Chen, *Angew Chem Int Edit*, 2012, **51**, 8021-8025.
31. D. Li, B. Mathew and C. B. Mao, *Small*, 2012, **8**, 3691-3697.
32. F. K. Wang, D. Li and C. B. Mao, *Adv Funct Mater*, 2008, **18**, 4007-4013.
33. D. Li, X. W. Qu, S. M. C. Newton, P. E. Klebba and C. B. Mao, *J Mater Chem*, 2012, **22**, 15702-15709.
34. T. H. Lim, D. McCarthy, S. C. Hendy, K. J. Stevens, S. A. Brown and R. D. Tilley, *Acs Nano*, 2009, **3**, 3809-3813.
35. J. M. Yuk, M. Jeong, S. Y. Kim, H. K. Seo, J. Kim and J. Y. Lee, *Chem Commun*, 2013, **49**, 11479-11481.
36. H. M. Zheng, R. K. Smith, Y. W. Jun, C. Kisielowski, U. Dahmen and A. P. Alivisatos, *Science*, 2009, **324**, 1309-1312.
37. K. Yonekura, S. Maki-Yonekura and K. Namba, *Nature*, 2003, **424**, 643-650.
38. M. A. Correa-Duarte, J. Pérez-Juste, A. Sánchez-Iglesias, M. Giersig and L. M. Liz-Marzán, *Angewandte Chemie International Edition*, 2005, **44**, 4375-4378.
39. C. B. Mao, D. J. Solis, B. D. Reiss, S. T. Kottmann, R. Y. Sweeney, A. Hayhurst, G. Georgiou, B. Iverson and A. M. Belcher, *Science*, 2004, **303**, 213-217.
40. E. Dujardin, C. Peet, G. Stubbs, J. N. Culver and S. Mann, *Nano Lett*, 2003, **3**, 413-417.
41. G. L. Wang and R. W. Murray, *Nano Lett*, 2004, **4**, 95-101.
42. H. Nakao, H. Shiigi, Y. Yamamoto, S. Tokonami, T. Nagaoka, S. Sugiyama and T. Ohtani, *Nano Lett*, 2003, **3**, 1391-1394.
43. Z. X. Deng, Y. Tian, S. H. Lee, A. E. Ribbe and C. D. Mao, *Angew Chem Int Edit*, 2005, **44**, 3582-3585.
44. J. Z. Chen, W. Y. Ko, Y. C. Yen, P. H. Chen and K. J. Lin, *Acs Nano*, 2012, **6**, 6633-6639.
45. N. Wan, J. Xu, G. R. Chen, X. H. Gan, S. H. Guo, L. Xu and K. J. Chen, *Acta Mater*, 2010, **58**, 3068-3072.
46. X. Wang, Q. Liu, S. Wu, B. Xu and H. Xu, *Adv. Mater.*, 2019, **31**, e1807716.
47. X. Zhang and L. D. Zhao, *J Materiomics*, 2015, **1**, 92-105.
48. D. Kraemer, Q. Jie, K. McEnaney, F. Cao, W. S. Liu, L. A. Weinstein, J. Loomis, Z. F. Ren and G. Chen, *Nature Energy*, 2016, **1**, 1-8.
49. D. D. Pineda, A. Rezaniakolaei, O. Brand, G. K. Fedder, C. Hierold, J. G. Korvink and O. Tabata, *Thermoelectric Energy Conversion: Basic Concepts and Device Applications*, Wiley, 2017.